Double-valued potential energy surface for H_2O derived from accurate *ab initio* data and including long-range interactions

João Brandão and Carolina M. A. Rio
Química–Faculdade de Ciências e Tecnologia, Universidade do Algarve–Campus de Gambelas, 8000-117 Faro, Portugal

(Received 18 March 2003; accepted 15 May 2003)

In a recent work we have been able to model the long-range interactions within the H_2O molecule. Using these long-range energy terms, a complete potential energy surface has been obtained by fitting high-quality *ab initio* energies to a double-valued functional form in order to describe the crossing between the two lowest-potential-energy surfaces. The two diabatic surfaces are represented using the double many-body expansion model, and the crossing term is represented using a three-body energy function. To warrant a coherent and accurate description for all the dissociation channels we have refitted the potential energy functions for the $H_2(^3\Sigma_u^+)$, $OH(^2\Pi)$, and $OH(^2\Sigma)$ diatomics. To represent the three-body extended Hartree–Fock nonelectrostatic energy terms, V_1, V_2, and V_{12}, we have chosen a polynomial on the symmetric coordinates times a range factor in a total of 148 coefficients. Although we have not used spectroscopic data in the fitting procedure, vibrational calculations, performed in this new surface using the DVR3D program suite, show a reasonable agreement with experimental data. We have also done a preliminary quasiclassical trajectory study (300 K). Our rate constant for the reaction $O(^1D)+H_2(^1\Sigma_g^+) \rightarrow OH(^2\Pi)+H(^2S)$, $k(300\ \mathrm{K})=(0.999\pm0.024)\times10^{-10}$ cm^3 molecule^{-1} s^{-1}, is very close to the most recent recommended value. This kinetic result reinforces the importance of the inclusion of the long-range forces when building potential energy surfaces. © *2003 American Institute of Physics.* [DOI: 10.1063/1.1589736]

I. INTRODUCTION

Although there have been a lot of recent studies on the potential energy surface (PES) for the $\tilde{X}\ ^1A_1$ ground state of the H_2O molecule,[1–7] the published potential energy surfaces do not equally cover the bottom of the well and the long-range part of the potential.

Mainly interested in the rovibrational spectra of water, the most recent potential energy surfaces do not reproduce the long-range interactions or use a simplified form to emulate them, neglecting "the intramolecular dependence of the atom–diatom dispersion coefficients" and the electrostatic quadrupole–quadrupole interaction between the O atom and H_2 diatom.

On the other hand, the $O(^1D)+H_2(^1\Sigma_g^+)\rightarrow OH(^2\Pi)+H(^2S)$ reaction, which occurs mainly in this system, is believed to have a null activation barrier. So the long-range forces between the O atom and H_2 diatomic should play an important role[8] in the dynamics of this important reaction in atmospheric and combustion chemistry.

Recently[9] we have been able to model the long-range interactions between the atoms and diatoms in their ground and first excited states as they appear as fragments in the water dissociation. The computed long-range coefficients, which are a function of the interaction angle and the interatomic distance of the diatomic, have been used to build potential energy functions to represent the electrostatic induction and dispersion energies within this system.

With this work, we aim to obtain an accurate potential energy surface for this system, covering all configurational space and the different dissociation channels allowed by spin and symmetry correlation as described by the following equations:

$$H_2O(\tilde{X}\ ^1A') \rightarrow \begin{cases} H_2(\tilde{X}\ ^1\Sigma_g^+)+O(^1D)\rightarrow 2H(^2S)+O(^1D), & \text{(i)} \\ H_2(\tilde{a}\ ^3\Sigma_u^+)+O(^3P)\rightarrow 2H(^2S)+O(^3P), & \text{(ii)} \\ OH(\tilde{A}\ ^2\Sigma)+H(^2S)\rightarrow 2H(^2S)+O(^1D), & \text{(i)} \\ OH(\tilde{X}\ ^2\Pi)+H(^2S)\rightarrow 2H(^2S)+O(^3P). & \text{(ii)} \end{cases} \quad (1)$$

To accomplish it, we used a double-valued functional form[10] to represent the two lowest $^1A_1$ surfaces. The adiabatic surfaces V_X and V_B are the two eigenvalues of a 2×2 matrix, where the diagonal terms are diabatic surfaces and the nondiagonal term represents the coupling between them. Due to the different dissociation channels and crossings of the upper sheet, this potential only reproduces accurately the ground-state potential energy surface, V_B being an approximation to the first excited state:

$$V_{X/B}=\begin{vmatrix} V_1 & V_{12} \\ V_{12} & V_2 \end{vmatrix} = \tfrac{1}{2}(V_1+V_2)\mp\tfrac{1}{2}\sqrt{(V_1-V_2)^2+4V_{12}^2}. \quad (2)$$

Each diabatic surface V_1 and V_2, is represented within the double many-body expansion (DMBE) framework[11] and the crossing term V_{12} is represented using a three-body en-

ergy function. According to the DMBE method each "many-body energy term" is divided as the sum of a short-range term called $V_{EHF,nele}$ ($nele$ stands for nonelectrostatic energy) and a long-range energy term V_{LR}. The first one accounts for the *extended* Hartree–Fock (EHF) energy, which includes the nondynamical correlation essential for the description of the bond dissociation. The second term includes the dynamic correlation energy, which appears in second-order perturbation theory. However, due to its long-range dependence, the electrostatic and induction energies are subtracted from the *extended* Hartree–Fock energy and included in the V_{LR} term. On the other hand, the intra- and inter-intra-atomic correlation terms, which depend on the superposition integrals, are included in the $V_{EHF,nele}$ energy term.

The three-body terms in this potential have been defined using accurate *ab initio* data from the literature. To cover some regions of the configurational space where there was a lack of information, we have also done *ab initio* multiconfigurational self-consistent-field (MCSCF) calculations using a triple-ζ basis set augmented with tight and diffuse functions.[12]

The quality of this new potential energy surface has been assessed with vibrational *ab initio* calculations and dynamical studies using quasiclassical trajectories (QCTs).

This article is organized as follows: Section II presents the diatomic potentials we have refitted from accurate *ab initio*[13,14] or Rydberg–Klein–Rees (RKR) spectroscopic data.[15] Section III a brief summary of the long-range interactions[9] used in this potential energy surface. Section IV describes the *ab initio* points and selection criteria as well as the functional form and numerical approach we used in the fitting procedure. In Sec. V we present a general overview of this surface. In Sec. VI we describe test calculations and comparison with experimental values: in Sec. VI A, preliminary QCT study at 300 K, and in Sec. VI B, the spectroscopic study we have done using the DVR3D suite of programs.[16] In Sec. VII we make some conclusions.

II. DIATOMIC POTENTIALS

To represent the four diatomic potentials resulting from the dissociation of the H_2O ground-state molecule, Eq. (1), we use the EHFACE2U potential model, method III.[17] Those potentials are constrained to satisfy a normalized kinetic field, and so they have a correct behavior at $R\rightarrow 0$. Also the V_{EHF} term has a correct asymptotic behavior at $R\rightarrow\infty$, reproducing the leading term for the exchange energy. They also have a dispersion energy term suitably damped.

However, as all the published potentials have different damping functions and functional forms, we have decided to use the diatomic potential for the $H_2(\tilde{X}\,^1\Sigma_g^+)$ (Ref. 17) and refitted three of them using the accurate *ab initio* results of Kołos and Wolniewicz[13,14] for the $H_2(\tilde{a}\,^3\Sigma_u^+)$ and the RKR experimental data points of Fallon *et al.*[15] for both OH ($^2\Pi$ and $^2\Sigma$) diatomic states. We need to use the same damping functions in order to get a coherent representation of the three-body exchange-dispersion energy terms.

The functional form we used to represent the diatomic potentials can be described by

$$V^{(2)}(R)=V_{EHF}^{(2)}(R)+V_{dc}^{(2)}(R), \tag{3}$$

where $V_{dc}^{(2)}$ is the usual dispersion correlation energy given by Eq. (4).[11,18] With the exception of the C_n values and the reduced coordinate ρ in the damping function χ_n, this term is the same for all diatomics:

$$V_{dc}^{(2)}(R)=-\sum_{n=6,8,10,\ldots} C_n\chi_n(R)R^{-n}. \tag{4}$$

In Eq. (4) we use the universal damping functions[11,18]

$$\chi_n(R)=\left[1-\exp\left(-\frac{A_nR}{\rho}-\frac{B_nR^2}{\rho^2}\right)\right]^n, \tag{5}$$

where

$$A_n=25.9528n^{-1.1868}, \tag{6}$$

$$B_n=15.7381\exp(-0.09729n), \tag{7}$$

and ρ is a reduced coordinate defined by

$$\rho=\tfrac{1}{2}(R_m+2.5R_0), \tag{8}$$

where R_m is the equilibrium diatomic geometry and R_0 is the Le Roy[19] parameter for the breakdown of the asymptotic expansion of the dispersion energy:

$$R_0(X-Y)=2(\langle r_X^2\rangle^{1/2}+\langle r_Y^2\rangle^{1/2}). \tag{9}$$

In contrast, the $V_{EHF}^{(2)}$ functional form has slight variations depending on the particular diatomic and their coefficients have been fitted to reproduce the total potential.

For the $H_2(^3\Sigma_u^+)$, we have used the accurate *ab initio* results of Kołos and Wolniewicz[13,14] to fit this potential. To represent the $V_{EHF}^{(2)}$ term we use the expression

$$V_{EHF}^{(2)}(R)=-DR^m\left(1+\sum_{i=1}^{3} a_iX^i\right)\exp\left[-\sum_{i=1}^{3} e_iX^i\right]+\chi_{exc}(R)V_{exc}^{asym}(R), \tag{10}$$

where $X=R-R_m$, R is the internuclear distance in the diatomic, R_m is the equilibrium internuclear distance, and V_{exc}^{asym} represents the asymptotic exchange energy. This last term is here the symmetric of the one for the singlet state,

$$V_{exc}^{asym}(R)=0.805R^{2.5}\exp(-2.0R), \tag{11}$$

and, similarly to the work of Varandas and Dias da Silva,[17] the asymptotic exchange energy is damped by the function χ_{exc}, which is approximated by the universal damping function [Eq. (5)] using $n=6$, χ_6.

In addition, to guide the potential at very short distances we have calculated two new points at the MCSCF level.

The calculations have been made using the suite programs GAMESS (Ref. 20) and augmented triple-ζ quality basis set: $(5s2p1d/3s2p1d)$ with diffuse $(1s1p1d)$ functions.[12] To compare our calculations with the literature results[13,14] we have made a set of calculations at other internuclear distances. In Fig. 1, we present seven points ($\triangle$) we have calculated. This figure shows the comparison with the literature data ($\bigcirc$). The two types of results are very close. The points we have used in the fitting procedure to obtain this diatomic potential are quoted in the Table I.

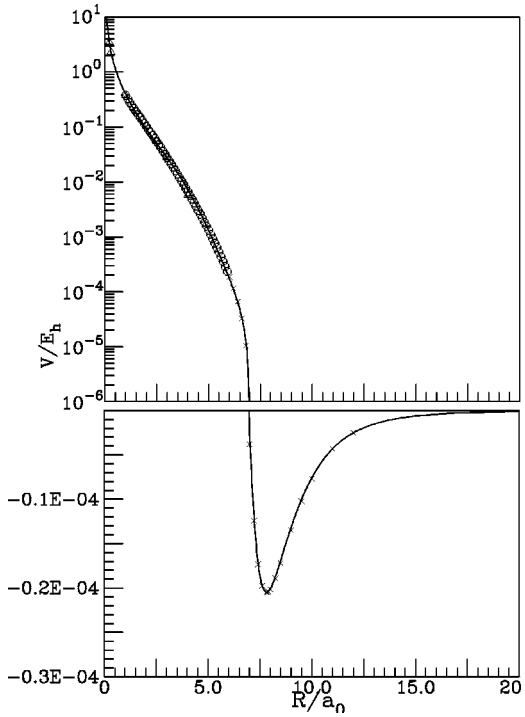

FIG. 1. Diatomic potential for H_2 molecule, $^3\Sigma_u^+$ state (solid line). Points: △, this work; ○, literature (Ref. 13), and ×, literature (Ref. 14).

The coefficients that define the complete potential for $H_2(^3\Sigma_u^+)$, Eqs. (4) and (10), are quoted in Table II, and Fig. 1 displays the potential.

For OH, states $^2\Pi$ and $^2\Sigma$, we have done a fitting procedure similar to that of Varandas and Voronin[21] to the RKR spectroscopic data.[15] The asymptotic exchange term has been taken from that work,[21] and the dispersion coefficients have been semiempirically estimated from polarizability data in a way similar to previous work.[9] For completeness, we display the functional form for the $V_{EHF}^{(2)}$ expression[21]

$$V_{EHF}^{(2)}(R) = -DR^m\left(1+\sum_{i=1}^{3} a_i X^i\right)\exp[-\gamma(R)X] + \chi_6(R)V_{exc}^{asym}(R), \tag{12}$$

where

$$\gamma(R) = \gamma_0[1+\gamma_1\tanh(\gamma_2 X)], \tag{13}$$

$$V_{exc}^{asym}(R) = -\tilde{A}R^{\tilde{\alpha}}(1+\tilde{a}R)\exp(-\tilde{\gamma}R), \tag{14}$$

TABLE I. Fitted points in the diatomic potential for the $H_2(^3\Sigma_u^+)$ molecule. In column *np* we present the number of the used points.

R/a_0	V/E_h	*np*
0.22	3.47321272[a]	1
0.30	2.30870248[a]	1
1.0↔5.9	Kołos and Wolniewicz[b]	50
6.0↔12.0	Kołos and Wolniewicz[c]	30

[a]This work.
[b]Reference 13.
[c]Reference 14.

TABLE II. Coefficients for the diatomic potential of $H_2(^3\Sigma_u^+)$.

Coefficients	$H_2(^3\Sigma_u^+)$	Coefficients	$H_2(^3\Sigma_u^+)$
D	2.64103167×10^{-5}	C_6	6.499027
a_1	1.4993695	C_8	124.3991
a_2	0.90948301	C_{10}	3285.828
a_3	0.20122436	C_{11}	−3475.0
e_1	2.90097680	C_{12}	1.215×10^5
e_2	0.47898562	C_{13}	-2.914×10^5
e_3	0.00274	C_{14}	6.061×10^6
R_0	6.928203	C_{15}	-2.305×10^7
R_m	7.820	C_{16}	3.938×10^8
ε	-2.04802401×10^{-5}		

and the remaining terms have the same meaning as in Eq. (10).

Table III quotes the parameters to use in Eqs. (12)–(14) for both states of the OH diatomic, and Fig. 2 shows the diatomic potential for the $OH(^2\Pi)$.

III. LONG-RANGE INTERACTIONS

An important feature of this new potential energy surface for H_2O is the ability to accurately reproduce the long-range interactions between the atoms and diatoms in their ground and first excited states as they appear as fragments in the water dissociation: see Eq. (1). The functional forms used to represent those interactions have been described elsewhere.[9]

As an example, we present in Fig. 3 a contour plot of the three-body electrostatic energy for an $O(^1D)$ atom around a $HH(^1\Sigma_g^+)$ diatomic.

IV. THREE-BODY EHF ENERGY TERMS

A. Input data

Using these long-range energy functions and the accurate diatomic potentials, the three-body EHF energy terms for V_1, V_2, and V_{12}, Eq. (2), have been obtained by fitting

TABLE III. Coefficients for diatomic potentials of OH molecule, states $^2\Pi$ and $^2\Sigma$.

Coefficients	$OH(^2\Pi)$	$OH(^2\Sigma)$
$-D$	0.240599442	0.103283115
a_1	2.4093609	3.0513954
a_2	1.1587677	1.8576639
a_3	0.53697044	1.4517489
γ_0	1.8450419	2.1847897
γ_1	2.7809326×10^3	4.5080859×10^3
γ_2	5.3432177×10^{-5}	5.346453×10^{-5}
m	−1	−1
$\tilde{A}$	0.307	1.022
$\tilde{\alpha}$	1.5	1.5
$\tilde{a}$	2.257329	−0.452055
$\tilde{\gamma}$	2.0	2.0
R_0	6.294894	6.334299622
R_m	1.8344	1.9086
C_6	10.00	10.34
C_8	180.45	306.8585254
C_{10}	3685.26	6328.709221
ε	−0.1701493	−0.0929757513

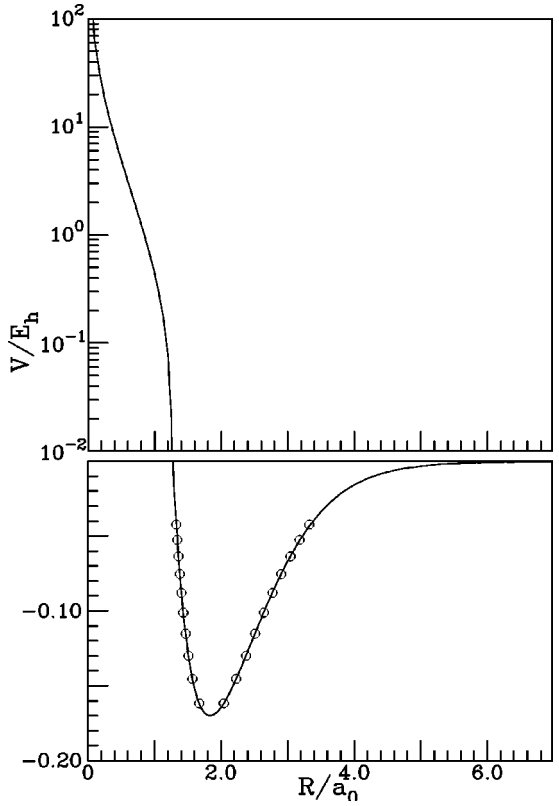

FIG. 2. Diatomic potential for OH molecule, $^2\Pi$ state (solid line). Fitted points (Ref. 15) ○.

total *ab initio* energies. Due to the importance of this system, there are a lot of *ab initio* results in this system. From the published data we decided to use those of Partridge and Schwenke,[4] Schneider, Giacomo, and Gianturco,[22] and Walch and Harding[23] which give a good database for the construction of the PES for the two lower singlet states energy of the H_2O molecule. Briefly:

(i) Points of Partridge and Schwenke, in 1997 (Ref. 4); calculations using a high-quality base set *cc-pV5Z*, increased with diffuse functions *s*, *p*, and *d* for the oxygen atom and *s* and *p* for the hydrogen atom. These points are henceforth assigned as set 1.

(ii) Points of Schneider, Giacomo, and Gianturco, in 1996 (Ref. 22); results gotten from a quality base set *triple-ζ*, increased with diffuse functions for the hydrogen and oxygen atoms. These points are henceforth assigned as set 2.

(iii) Points of Walch and Harding, in 1988 (Ref. 23); results obtained from different contractions of the ANO base set (*atomic natural orbitals*). These points are henceforth assigned as set 3.

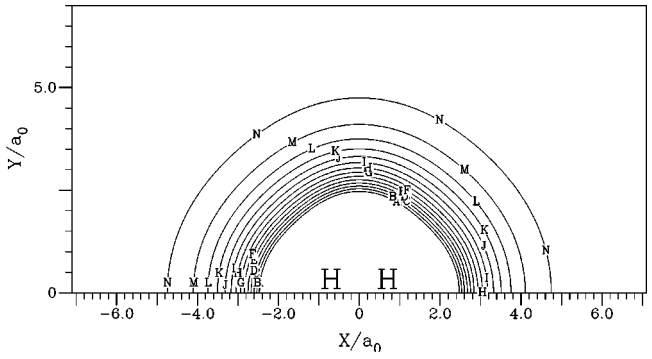

FIG. 3. Contour of three-body electrostatic energy for O(^1D) atom around the HH($^1\Sigma_g^+$) diatomic, $V_{ele}^{(3)}$. The diatomic has been fixed at the internuclear distance $1.401a_0$, with the geometric center in the origin. The contours are spaced by $0.5mE_h$ and the beginning $-7.0mE_h$(O=$0.0mE_h$). In this figure, and in the remaining ones, *X* and *Y* are the Cartesian coordinates of the moving atom.

All these calculations include the dynamic correlation. Moreover, these energies have been semiempirically corrected by the scaled external correlation method[24] (SEC) to account for the incompleteness of the basis set and higher-order excitation terms.

To minimize the possible inconsistencies between the different sets of data we decided to start from the high-quality points of set 1. We have discarded the points of sets 2 and 3 whose ''distance'' to any point of set 1 was less than $0.5a_0$. A similar criterion has been used for sets 2 and 3. In cases where this ''distance'' is lower than $0.5a_0$ only the points of set 3 have been considered. By ''distance'' between two points *i* and *j*, D^{ij}, we mean the result of the expression

$$D^{ij}=\sqrt{\sum_{k=1}^{3}[(R_k^i-R_k^j)^2]}. \tag{15}$$

Also to avoid inconsistencies with our accurate long-range energy term,[9] we have discarded those points whose configuration has at least one interatomic distance R_1, R_2, or R_3 greater than $5.5a_0$.

As the authors have published only the total interaction energies, the three-body *extended* Hartree–Fock nonelectrostatic term $V_{EHF,nele}^{(3)}$ was obtained from the total energy for this system subtracting the two-body terms and the three-body dynamic correlation energy as well as the electrostatic and induction energies as modeled in our previous work.[9]

In regions not covered by those *ab initio* points we have computed some additional points at the MCSCF level. These calculations have been made with the suite programs GAMESS (Ref. 20) and using a augmented triple-ζ quality basis set: the above referred basis set for the H atom and $(10s5p3d1f/4s3p2d1f)$ augmented with tight functions $(2s2p1d)$ and diffuse $(1s1p1d1f)$ for the O atom.[25] To define the active space for the multiconfiguration calculations we have used all the molecular orbitals generated from the 1*s* and 2*s* orbitals of H atom and 1*s*, 2*s*, 2*p*, 3*s*, and 3*p* orbitals of the O atom. We have considered all configurations generated within this space. Test calculations have shown that a MCSCF calculation within this active space gives lower energy values than a MR–CI (multireference configuration-interaction) with a smaller active space but larger external orbitals. Those points have been corrected to account for the basis-set superposition error.[26]

B. Fitting procedure

The ground state $X\,^1A'$ and the first excited state $B\,^1A'$ of the water molecule are here defined as the eigenvalues of

TABLE IV. Origin and number of *ab initio* points selected for each component and global potential.

	Set 1[a]	Set 2[b]	Set 3[c]	This work	Total
V_1	501	152	78	1	732
V_2	103	155	21	43	322
V_X	184	29	33	-	246
V_B	-	27	-	-	27
Total	788	363	132	44	1327

[a]Reference 4.
[b]Reference 22.
[c]Reference 23.

a 2×2 matrix. They correspond to two adiabatic surfaces V_X and V_B represented by the double-valued functional form, Eq. (2). These adiabatic surfaces are computed from the diabatic surfaces V_1 and V_2 and the crossing term V_{12} that couples them.

Following the work of Murrell *et al.*,[10] for the H_2O molecule we can write the two diabatic surfaces

$$\begin{aligned} V_1 &= V_{\mathrm{O}}^{(1)}(^1D) + V_{\mathrm{OH}}^{(2)}(^2\Sigma, \mathrm{R}_2) + V_{\mathrm{OH}}^{(2)}(^2\Sigma, \mathrm{R}_3) \\ &\quad + V_{\mathrm{HH}}^{(2)}(^1\Sigma_g^+, \mathrm{R}_1) + V_{1(LR)}^{(3)}(\mathbf{R}) + V_{1(EHF,nele)}^{(3)}(\mathbf{R}), \\ V_2 &= V_{\mathrm{OH}}^{(2)}(^2\Pi, \mathrm{R}_2) + V_{\mathrm{OH}}^{(2)}(^2\Pi, \mathrm{R}_3) + V_{\mathrm{HH}}^{(2)}(^3\Sigma_u^+, \mathrm{R}_1) \\ &\quad + V_{2(LR)}^{(3)}(\mathbf{R}) + V_{2(EHF,nele)}^{(3)}(\mathbf{R}), \\ V_{12} &= V_{12(EHF,nele)}^{(3)}(\mathbf{R}), \end{aligned} \tag{16}$$

where $V_{I(EHF,nele)}^{(3)}$ (with $I=1$, 2, and 12) are the different three-body nonelectrostatic EHF energies terms, and $V_{1(LR)}^{(3)}$ and $V_{2(LR)}^{(3)}$ represent the sum of $V_{ind}^{(3)}$, $V_{ele}^{(3)}$, and $V_{dc}^{(3)}$ (previously defined for each diabatic surface V_1 and V_2).

In order to define the two adiabatic surfaces (V_X and V_B), we need to fit three terms: the diabatic surfaces V_1 and V_2 and the crossing term V_{12}. We used the following procedure:

(i) We used the description of the PES of Murrell *et al.*[10] to define the crossing regions.
(ii) We considered that in regions far from the crossing, the diabatic surfaces coincide with the adiabatic surfaces.
(iii) We attributed each *ab initio* point to the diabatic surfaces V_1 and V_2. Whenever the point is located near to the crossing region, where the term of coupling V_{12} is significant, it will be attributed directly to the surface V_X or V_B.
(iv) We have done a preliminary study on the diabatic surfaces V_1 and V_2 in order to define the number of parameters necessary to get a good fit. Whenever necessary we have computed additional points.
(v) Those preliminary parameters have been used as a starting point for a global fitting where the points attributed
  (a) directly to the V_1 (or V_2) diabatic surface were used to fit the function that defines the V_1 (or V_2) surface and would take value of zero in the fitting to the V_{12} term and
  (b) to the V_X (or V_B) adiabatic surface were used to fit the function that defines the V_X (or V_B) surface, that includes the V_1 and V_2 functions and the coupling term V_{12}.

As described above, we have verified that in some regions the information was insufficient to define the true behavior of the surface and we carried out some calculations for the H_2O system. We refer, in particular, the V_2 diabatic surface and the united atom limit on the V_1 surface. In this last case we have estimated the three-body $V_{EHF,nele}$ energy term from the energy of the united atom limit of O+H+H (Ne atom) subtracting the energy of the diatomics united atoms (two F atoms and one He atom). All these calculations have been done using a basis set with similar quality and using the same active space as for H_2O.

Table IV presents the *ab initio* points used in the building of this potential energy surface. As an example, we display in Fig. 4 the distribution points used in this fitting for the C_{2v} insertion of the O atom in the H_2 diatomic.

The functional form used to represent the nonelectrostatic three-body terms, for each term of this potential energy surface, $V_{I,I=1,2,12}$, can be presented by a product of a polynomial form using symmetry coordinates (Q_1, Q_2, and Q_3),[27] $\mathbf{P}$, with a range factor $\mathbf{D}$:

$$\begin{aligned} V_{I(EHF,nele)}^{(3)}(R_1,R_2,R_3) &= \mathbf{P}_I^{(3)}(Q_1,Q_2,Q_3) \\ &\quad \times \mathbf{D}_I^{(3)}(R_1,R_2,R_3). \end{aligned} \tag{17}$$

The use of the D_{3h} symmetry coordinates is an easy way to include the permutation symmetry of the H_2O system on

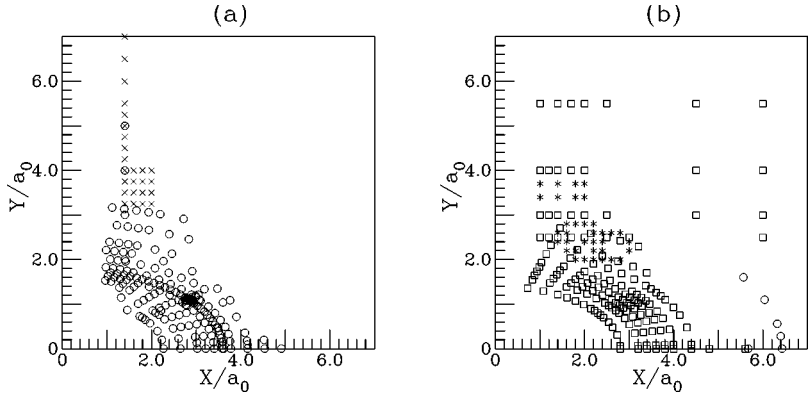

FIG. 4. Points distribution used in surfaces V_1 and V_2 calibration for the insertion C_{2v} of the O atom in the H_2 diatomic: (a) surface V_1 and (b) surface V_2. Legend: ○, set 1 (Ref. 4); ×, set 3 (Ref. 23); □, set 2 (Ref. 22), and ∗, this work.

the potential energy function. For a system with S_2 permutation symmetry the polynomials must use only products and powers of the integrity base

$$Q_1,\ Q_3,\ S_{2a}^2,\ S_{2b}^2,\ \text{and}\ S_3^3,$$

where

$$\begin{bmatrix} Q_1(A_1') \\ Q_2(E') \\ Q_3(E') \end{bmatrix} = \begin{bmatrix} \sqrt{1/3} & \sqrt{1/3} & \sqrt{1/3} \\ 0 & \sqrt{1/2} & -\sqrt{1/2} \\ \sqrt{2/3} & -\sqrt{1/6} & -\sqrt{1/6} \end{bmatrix} \begin{bmatrix} R_1-R_1^{(i)} \\ R_2-R_2^{(i)} \\ R_3-R_3^{(i)} \end{bmatrix}, \tag{18}$$

$$\begin{aligned} S_{2a}^2 &= Q_2^2+Q_3^2, \\ S_{2b}^2 &= Q_2^2-Q_3^2, \\ S_3^3 &= Q_3^3-3Q_2^2Q_3, \end{aligned} \tag{19}$$

and $R_1^{(i)}$, $R_2^{(i)}$, and $R_3^{(i)}$ are a reference geometry for each potential term, whose values are quoted in Table V. For V_1 we used as reference the equilibrium position of the water molecule; for V_2 and V_{12} we found convenient to use C_{2v} geometries whose perimeter is close to the region where those terms should play an important role.

TABLE V. Reference geometries used on the different elements of matrix V.

V_i	$R_1^{(i)}$	$R_2^{(i)}$	$R_3^{(i)}$
V_1	2.86194	1.80965	1.80965
V_2	4.04	2.717	2.717
V_{12}	3.0	2.6	2.6

We considered it convenient to use polynomials of degree 8 (95 terms), 5 (34 terms), and 3 (13 terms) for the components V_1, V_2, and V_{12}, respectively, in order to get an accurate fit avoiding any nonrealistic behavior in regions not covered by the *ab initio* data. These polynomial terms, used to define the three-body EHF terms, are indicated in the Eqs. (20), (21), and (22):

$$\begin{aligned} P_{1(EHF,nele)}^{(3)} = {} & c_1+c_2Q_1+c_3Q_3+c_4Q_1^2+c_5S_{2a}^2+c_6Q_1Q_3+c_7S_{2b}^2+c_8Q_1^3+c_9Q_1S_{2a}^2+c_{10}S_3^3+c_{11}Q_1^2Q_3+c_{12}Q_1S_{2b}^2 \\ & +c_{13}Q_3S_{2a}^2+c_{14}Q_1^4+c_{15}Q_1^2S_{2a}^2+c_{16}S_{2a}^4+c_{17}Q_1S_3^3+c_{18}Q_1^3Q_3+c_{19}Q_1^2S_{2b}^2+c_{20}Q_1Q_3S_{2a}^2+c_{21}Q_3S_3^3 \\ & +c_{22}S_{2a}^2S_{2b}^2+c_{23}Q_1^5+c_{24}Q_1^3S_{2a}^2+c_{25}Q_1S_{2a}^4+c_{26}Q_1^2S_3^3+c_{27}S_{2a}^2S_3^3+c_{28}Q_1^4Q_3+c_{29}Q_1^3S_{2b}^2+c_{30}Q_1^2Q_3S_{2a}^2 \\ & +c_{31}Q_1Q_3S_3^3+c_{32}Q_1S_{2a}^2S_{2b}^2+c_{33}Q_3S_{2a}^4+c_{34}S_{2b}^2S_3^3+c_{35}Q_1^6+c_{36}Q_1^4S_{2a}^2+c_{37}Q_1^2S_{2a}^4+c_{38}Q_1^3S_3^3 \\ & +c_{39}Q_1S_3^3S_{2a}^2+c_{40}S_{2a}^6+c_{41}S_3^6+c_{42}Q_1^5Q_3+c_{43}Q_1^4S_{2b}^2+c_{44}Q_1^3Q_3S_{2a}^2+c_{45}Q_1^2Q_3S_3^3+c_{46}Q_1^2S_{2a}^2S_{2b}^2 \\ & +c_{47}Q_1Q_3S_{2a}^2 2+c_{48}Q_1S_3^3S_{2b}^2+c_{49}Q_3S_{2a}^2S_3^3+c_{50}S_{2b}^2S_{2a}^4+c_{51}Q_1^7+c_{52}Q_1^5S_{2a}^2+c_{53}Q_1^3S_{2a}^4+c_{54}Q_1^4S_3^3 \\ & +c_{55}Q_1^2S_{2a}^2S_3^3+c_{56}Q_1S_{2a}^6+c_{57}Q_1S_3^6+c_{58}S_3^3S_{2a}^4+c_{59}Q_3Q_1^6+c_{60}Q_3Q_1^4S_{2a}^2+c_{61}Q_3Q_1^2S_{2a}^4+c_{62}Q_1^3Q_3S_3^3 \\ & +c_{63}Q_1Q_3S_3^3S_{2a}^2+c_{64}Q_3S_{2a}^6+c_{65}Q_3S_3^6+c_{66}Q_1^5S_{2b}^2+c_{67}Q_1^3S_{2a}^2S_{2b}^2+c_{68}Q_1^2S_3^3S_{2b}^2+c_{69}Q_1S_{2a}^4S_{2b}^2 \\ & +c_{70}S_3^3S_{2a}^2S_{2b}^2+c_{71}Q_1^8+c_{72}Q_1^6S_{2a}^2+c_{73}Q_1^4S_{2a}^4+c_{74}Q_1^5S_3^3+c_{75}Q_1^3S_3^3S_{2a}^2+c_{76}Q_1^2S_{2a}^6+c_{77}Q_1^2S_3^6 \\ & +c_{78}Q_1S_3^3S_{2a}^4+c_{79}S_{2a}^8+c_{80}S_3^6S_{2a}^2+c_{81}Q_1^7Q_3+c_{82}Q_1^5Q_3S_{2a}^2+c_{83}Q_1^3Q_3S_{2a}^4+c_{84}Q_1^4S_3^6+c_{85}Q_1^2S_3^6S_{2a}^2 \\ & +c_{86}Q_1Q_3S_{2a}^6+c_{87}Q_1Q_3S_3^6+c_{88}Q_1^6S_{2b}^2+c_{89}Q_1^4S_{2b}^2S_{2a}^2+c_{90}Q_1^3S_3^3S_{2b}^2+c_{91}Q_1^2S_{2a}^4S_{2b}^2+c_{92}Q_1S_3^3S_{2b}^2S_{2a}^2 \\ & +c_{93}Q_3S_3^3S_{2a}^4+c_{94}S_3^6S_{2b}^2+c_{95}S_{2a}^6S_{2b}^2, \end{aligned} \tag{20}$$

$$\begin{aligned} P_{2(EHF,nele)}^{(3)} = {} & c_{98}+c_{99}Q_1+c_{100}Q_3+c_{101}Q_1^2+c_{102}S_{2a}^2+c_{103}Q_1Q_3+c_{104}S_{2b}^2+c_{105}Q_1^3+c_{106}Q_1S_{2a}^2+c_{107}S_3^3+c_{108}Q_1^2Q_3 \\ & +c_{109}Q_1S_{2b}^2+c_{110}Q_3S_{2a}^2+c_{111}Q_1^4+c_{112}Q_1^2S_{2a}^2+c_{113}S_{2a}^4+c_{114}Q_1S_3^3+c_{115}Q_1^3Q_3+c_{116}Q_1^2S_{2b}^2 \\ & +c_{117}Q_1Q_3S_{2a}^2+c_{118}Q_3S_3^3+c_{119}S_{2a}^2S_{2b}^2+c_{120}Q_1^5+c_{121}Q_1^3S_{2a}^2+c_{122}Q_1S_{2a}^4+c_{123}Q_1^2S_3^3+c_{124}S_{2a}^2S_3^3 \\ & +c_{125}Q_1^4Q_3+c_{126}Q_1^3S_{2b}^2+c_{126}Q_1^3S_{2b}^2+c_{127}Q_1^2Q_3S_{2a}^2+c_{128}Q_1Q_3S_3^3+c_{129}Q_1S_{2a}^2S_{2b}^2+c_{130}Q_3S_{2a}^4 \\ & +c_{131}S_{2b}^2S_3^3, \end{aligned} \tag{21}$$

$$\begin{aligned} P_{12(EHF,nele)}^{(3)} = {} & c_{134}+c_{135}Q_1+c_{136}Q_3+c_{137}Q_1^2+c_{138}S_{2a}^2+c_{139}Q_1Q_3+c_{140}S_{2b}^2+c_{141}Q_1^3+c_{142}Q_1S_{2a}^2+c_{143}S_3^3+c_{144}Q_1^2Q_3 \\ & +c_{145}Q_1S_{2b}^2+c_{146}Q_3S_{2a}^2. \end{aligned} \tag{22}$$

TABLE VI. Coefficients for the three-body *extended* Hartree–Fock energy $V^{(3)}_{1(EHF,nele)}$ term.

$c_1=-1.565690230\times10^{-1}$	$c_{34}=1.755636267\times10^{-2}$	$c_{67}=-2.015458742\times10^{-1}$
$c_2=-2.544931663\times10^{-1}$	$c_{35}=-4.571252263\times10^{-2}$	$c_{68}=6.721735197\times10^{-2}$
$c_3=-4.876804350\times10^{-2}$	$c_{36}=1.272353899\times10^{-2}$	$c_{69}=1.712406839\times10^{-1}$
$c_4=-2.690037685\times10^{-1}$	$c_{37}=-1.199479525\times10^{-1}$	$c_{70}=6.228997124\times10^{-2}$
$c_5=-1.535865259\times10^{-3}$	$c_{38}=9.468891942\times10^{-2}$	$c_{71}=-3.420843299\times10^{-4}$
$c_6=-4.890066230\times10^{-2}$	$c_{39}=-2.616965983\times10^{-2}$	$c_{72}=1.340173021\times10^{-2}$
$c_7=-7.329374732\times10^{-2}$	$c_{40}=-6.339820029\times10^{-2}$	$c_{73}=-4.185837518\times10^{-2}$
$c_8=-2.109344267\times10^{-1}$	$c_{41}=-4.934658276\times10^{-2}$	$c_{74}=-1.143824325\times10^{-2}$
$c_9=-6.445301047\times10^{-2}$	$c_{42}=3.225361439\times10^{-2}$	$c_{75}=3.392045669\times10^{-2}$
$c_{10}=2.411710888\times10^{-2}$	$c_{43}=7.834891306\times10^{-2}$	$c_{76}=8.324394198\times10^{-2}$
$c_{11}=-1.555868493\times10^{-2}$	$c_{44}=-4.235299197\times10^{-2}$	$c_{77}=-8.282447683\times10^{-3}$
$c_{12}=-5.607487072\times10^{-2}$	$c_{45}=-8.355138053\times10^{-2}$	$c_{78}=-7.865970804\times10^{-2}$
$c_{13}=6.202541496\times10^{-2}$	$c_{46}=-2.899296365\times10^{-1}$	$c_{79}=-2.481027858\times10^{-2}$
$c_{14}=-1.429634757\times10^{-1}$	$c_{47}=1.331932799\times10^{-1}$	$c_{80}=-1.354741296\times10^{-2}$
$c_{15}=-7.444150867\times10^{-2}$	$c_{48}=-5.167976333\times10^{-2}$	$c_{81}=-5.307323810\times10^{-3}$
$c_{16}=6.156263566\times10^{-2}$	$c_{49}=-2.347859542\times10^{-2}$	$c_{82}=-9.247430789\times10^{-3}$
$c_{17}=-2.245935938\times10^{-3}$	$c_{50}=-1.777711260\times10^{-2}$	$c_{83}=2.436516685\times10^{-2}$
$c_{18}=1.330353546\times10^{-2}$	$c_{51}=-1.299842803\times10^{-2}$	$c_{84}=-3.674205193\times10^{-3}$
$c_{19}=-6.788598952\times10^{-2}$	$c_{52}=2.970783506\times10^{-2}$	$c_{85}=3.402165882\times10^{-3}$
$c_{20}=2.271341007\times10^{-3}$	$c_{53}=-7.347156570\times10^{-2}$	$c_{86}=1.899518378\times10^{-2}$
$c_{21}=8.980070809\times10^{-3}$	$c_{54}=7.465634301\times10^{-3}$	$c_{87}=-1.741461802\times10^{-2}$
$c_{22}=-4.986636030\times10^{-2}$	$c_{55}=9.699947247\times10^{-3}$	$c_{88}=1.174832037\times10^{-3}$
$c_{23}=-8.429336120\times10^{-2}$	$c_{56}=1.649570767\times10^{-1}$	$c_{89}=-5.667240702\times10^{-2}$
$c_{24}=8.978555840\times10^{-3}$	$c_{57}=3.481731649\times10^{-2}$	$c_{90}=-7.274439089\times10^{-3}$
$c_{25}=3.568207396\times10^{-2}$	$c_{58}=6.307806127\times10^{-2}$	$c_{91}=9.909591032\times10^{-2}$
$c_{26}=7.898108250\times10^{-2}$	$c_{59}=5.148261697\times10^{-3}$	$c_{92}=-7.952480341\times10^{-2}$
$c_{27}=-3.299218814\times10^{-3}$	$c_{60}=-6.304245065\times10^{-2}$	$c_{93}=-3.072103204\times10^{-3}$
$c_{28}=2.266503020\times10^{-2}$	$c_{61}=6.882370932\times10^{-2}$	$c_{94}=1.970459378\times10^{-3}$
$c_{29}=4.924099395\times10^{-2}$	$c_{62}=4.033730863\times10^{-2}$	$c_{95}=-2.362856551\times10^{-2}$
$c_{30}=-6.192243909\times10^{-2}$	$c_{63}=2.565541551\times10^{-2}$	$c_{96}=8.0\times10^{-1}$[a]
$c_{31}=1.006236871\times10^{-2}$	$c_{64}=-6.078121832\times10^{-2}$	$c_{97}=1.0$[a]
$c_{32}=-1.067837639\times10^{-1}$	$c_{65}=-2.962569550\times10^{-2}$	
$c_{33}=1.965447873\times10^{-2}$	$c_{66}=3.084390610\times10^{-2}$	

[a]This coefficient has been fixed (not fitted).

TABLE VII. Coefficients for the three-body *extended* Hartree–Fock energy $V^{(3)}_{2(EHF,nele)}$ term.

$c_{98}=1.208067587\times10^{-1}$	$c_{110}=5.333761656\times10^{-2}$	$c_{122}=-1.519678996\times10^{-2}$
$c_{99}=-3.461573091\times10^{-2}$	$c_{111}=-1.313796927\times10^{-2}$	$c_{123}=-2.608303613\times10^{-2}$
$c_{100}=-3.750302864\times10^{-2}$	$c_{112}=5.581602062\times10^{-2}$	$c_{124}=-2.439369041\times10^{-3}$
$c_{101}=-1.024072632\times10^{-1}$	$c_{113}=8.072039816\times10^{-3}$	$c_{125}=-3.230616849\times10^{-4}$
$c_{102}=3.886559362\times10^{-3}$	$c_{114}=3.448517557\times10^{-2}$	$c_{126}=-1.622479086\times10^{-2}$
$c_{103}=-5.565028247\times10^{-2}$	$c_{115}=-1.509775116\times10^{-2}$	$c_{127}=4.314598580\times10^{-2}$
$c_{104}=-1.387475546\times10^{-1}$	$c_{116}=6.871987343\times10^{-3}$	$c_{128}=3.349953640\times10^{-2}$
$c_{105}=-5.669833170\times10^{-2}$	$c_{117}=4.548979350\times10^{-2}$	$c_{129}=1.267395642\times10^{-2}$
$c_{106}=8.381138633\times10^{-2}$	$c_{118}=8.392592250\times10^{-4}$	$c_{130}=3.163071652\times10^{-3}$
$c_{107}=2.316598891\times10^{-3}$	$c_{119}=2,332029125\times10^{-2}$	$c_{131}=5.184081419\times10^{-3}$
$c_{108}=-4.894908326\times10^{-2}$	$c_{120}=-1.285789631\times10^{-3}$	$c_{132}=8.0\times10^{-1}$[a]
$c_{109}=-8.779017665\times10^{-2}$	$c_{121}=-1.553370286\times10^{-2}$	$c_{133}=1.0$[a]

[a]This coefficient has been fixed (not fitted).

TABLE VIII. Coefficients for the three-body *extended* Hartree–Fock energy $V^{(3)}_{12(EHF,nele)}$ term.

$c_{134}=-1.058457775\times10^{-1}$	$c_{139}=1.103968854\times10^{-1}$	$c_{144}=-1.888672360\times10^{-1}$
$c_{135}=-2.059102604\times10^{-2}$	$c_{140}=5.152243701\times10^{-2}$	$c_{145}=-1.251485382\times10^{-1}$
$c_{136}=6.661037391\times10^{-2}$	$c_{141}=7.878724664\times10^{-2}$	$c_{146}=-7.811582863\times10^{-2}$
$c_{137}=-6.610026832\times10^{-2}$	$c_{142}=8.313253687\times10^{-2}$	$c_{147}=7.702019726\times10^{-9}$
$c_{138}=1.843067372\times10^{-2}$	$c_{143}=-2.827314866\times10^{-2}$	$c_{148}=3.652832367\times10^{-1}$

TABLE IX. Minimum C_{2v} for the water molecule.

Prop.	This work	PJT[a]	PS1[b]	PS2[c]	Expt.[d]
R_{HH}	2.860831	2.86261719	2.86185923	2.86156774	2.86193768
R_{OH}	1.809798	1.81020726	1.81158582	1.80977168	1.80965
∠HOH	104.4407	104.499647	104.348	104.481	104.51008

[a]Reference 2.
[b]Reference 4, only considering the *ab initio* fit.
[c]Reference 4, considering the total potential.
[d]See Refs. 16 and 21 from Murrell *et al.* (Ref. 10).

The decay functions we used in terms V_1 [Eq. (23)] and V_2 [Eq. (24)] are the usual product of hyperbolic tangent functions. However, the decay for the V_{12} term [Eq. (25)] deserves special attention: instead of a hyperbolic tangent we have used Gaussian functions to cancel this term far from the interest region; for collinear configurations the two diabatic surfaces correlate with states of different symmetry and the coupling term should be zero, which is accomplished with the term $\sin(\angle HOH)$ in Eq. (25); the coupling strength being dependent on the difference between the diabatic surfaces, we have included a Gaussian term function of that difference:

$$D_1^{(3)}(\mathbf{R}) = \{1-\tanh[(R_1-R_1^{(1)})c_{96}]\}\{1-\tanh[(R_2 - R_2^{(1)})c_{97}]\}\{1-\tanh[(R_3-R_3^{(1)})c_{97}]\}, \quad (23)$$

$$D_2^{(3)}(\mathbf{R}) = \{1-\tanh[(R_1-R_1^{(2)})c_{132}]\}\{1-\tanh[(R_2 - R_2^{(2)})c_{133}]\}\{1-\tanh[(R_3-R_3^{(2)})c_{133}]\}, \quad (24)$$

$$D_{12}^{(3)}(\mathbf{R}) = \sin(\angle HOH)\exp[-100(V_1-V_2)^2] \times \exp[-c_{147}((R_1-R_1^{(12)})^2)] \times \exp[-c_{148}((R_2+R_3-2R_3^{(12)})^2)]. \quad (25)$$

Similar to the definition of the symmetry coordinates Q_i, in Eq. (18), in the decay functions (23), (24), and (25) we use a displacement from the same reference geometry.

To warrant a good description to the region closed to the equilibrium geometry of the water molecule, we used a general weighting function, Eq. (26), to the points assigned to V_1, where $\tilde{w}$ and E_{ref} assume the values 6000 and $0.3704E_h$, respectively:

$$W_i = \frac{\tilde{w}}{\sqrt{E_i+E_{ref}}+0.001}. \quad (26)$$

TABLE X. Spectroscopic properties for the water molecule.

Prop.	This work	Expt.[a]
D_e	−0.370401	−0.3704
F_{11}	0.542449	0.542747
$F_{\alpha\alpha}$	0.162052	0.160559
F_{12}	-0.292350×10^{-2}	-0.6423×10^{-2}
$F_{1\alpha}$	0.314402×10^{-1}	0.26703×10^{-1}

[a]See Refs. 16 and 21 from Murrell *et al.* (Ref. 10).

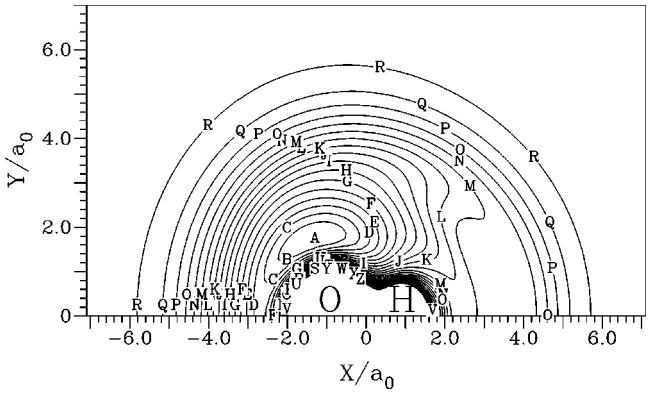

FIG. 5. Contour plot of diabatic surfaces V_1 in H_2O molecule, for H atom moving around an OH ($1.7444a_0 \leqslant R_{O-H} \leqslant 1.9444a_0$) and the center of the bond fixed at the origin. Contours are equally spaced by $0.02E_h$, starting at $-0.3704E_h$.

Additionally, we multiply this weight by a factor of 200 if the configuration is close to this minimum—i.e., if it satisfies the condition expressed by Eq. (27):

$$\sqrt{\sum_{i=1}^{3}[(R_i-R_i^{(1)})^2]} < 0.5a_0. \quad (27)$$

Similarly, for the points assigned to V_2, V_X, V_B, and V_{12} we used Eq. (26) where $\tilde{w}$ assumes the values 50, 100, 1, and 10, respectively. Only for V_2 points has the value of E_{ref} been changed to $0.172E_h$. This value corresponds to the average between the minimum of two diatomics, $H_2(^1\Sigma_g^+)$ and $OH(^2\Pi)$, respectively, $0.17447E_h$ and $0.1702E_h$. During the fitting procedure special weights have been assigned to selected points.

The coefficient values we have obtained on the final fit are quoted in Tables VI, VII, and VIII.

V. GENERAL OVERVIEW OF A NEW PES

In Table IX we present the geometry of the stable minimum of the water molecule, obtained from this surface and from some of the most recent published potentials. Table X quotes the force constants of this potential. Both tables com-

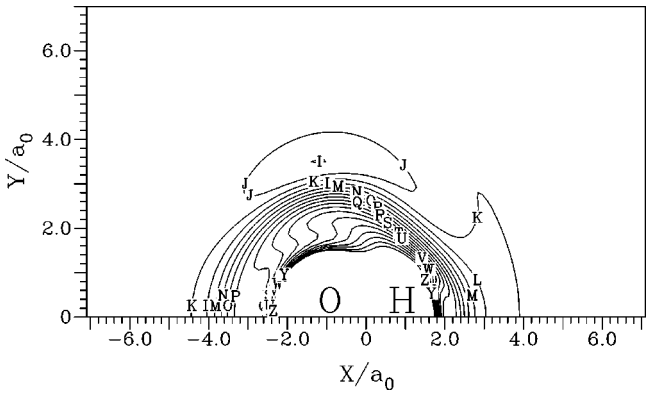

FIG. 6. Contour plot of diabatic surface V_2 in H_2O molecule, for H atom moving around an OH ($1.7444a_0 \leqslant R_{O-H} \leqslant 1.9444a_0$) and the center of the bond fixed at the origin. Contours are equally spaced by $0.02E_h$, starting at $-0.3704E_h$.

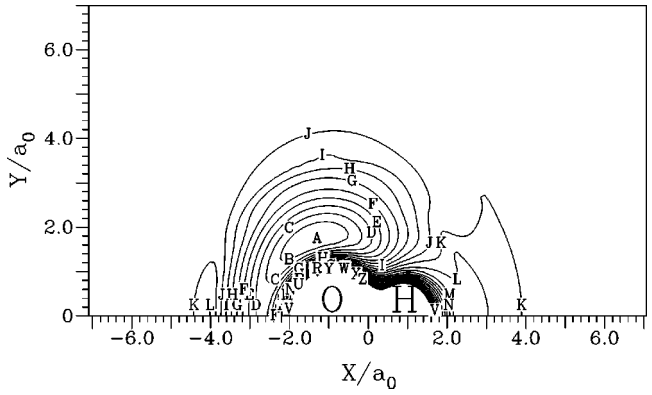

FIG. 7. Contour plot of H_2O ($X\,^1A'$) new PES, for H atom moving around an OH ($1.7444a_0 \leqslant R_{O-H} \leqslant 1.9444a_0$) and the center of the bond fixed at the origin. Contours are equally spaced by $0.02E_h$, starting at $-0.3704E_h$.

pare the predicted values with experiment showing a good agreement. Note that this potential and the entry under PS1 don't use any experimental data in their calibration.

Figures 5 and 6 show the contour plots for the V_1 and V_2 diabatic surfaces, for a H atom moving around an equilibrium OH molecule, while Figs. 7 and 8 plot the same configuration for the adiabatic surfaces X and B, respectively. A perspective view for this configuration on the ground state surface is shown in Fig. 9. From these figures the crossing between these diabatic surfaces is apparent particularly at the collinear geometries where the coupling term vanishes. It is important to notice the saddle point for the isomerization of H_2O, 11 346 cm^{-1} above the bottom well (this value does not include any correction: see point (1) in Table XI), which plays an important role in the vibrational spectra and dynamics of a high-energy H_2O molecule.[28] This point is best viewed as a minimum in Fig. 10 where we plot the collinear stretching of the two H atoms on the ground-state surface. This figure clearly shows the crossing at these geometries of surface V_1, $H_2O(^1\Sigma^+)$ state, shown in Fig. 11 and surface V_2, $H_2O(^1\Pi)$ state, shown in Fig. 12. Point (2) of the above referred table, shown in Figs. 10 and 12 as a minimum, is also a saddle point for the isomerization for large OH values, on a van der Waals region of the $H_2O(^1\Pi)$ surface before the

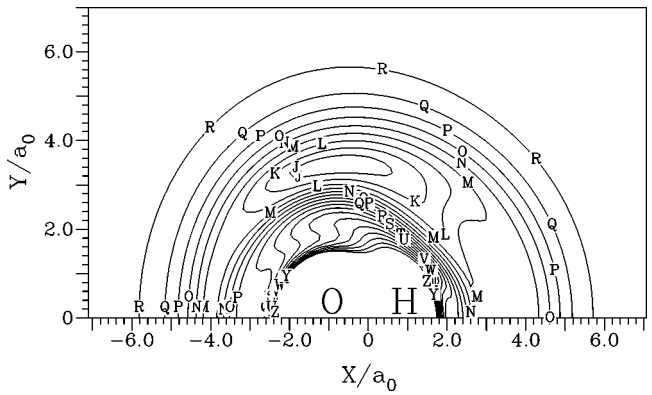

FIG. 8. Contour plot of H_2O ($B\,^1A'$) new PES, for H atom moving around an OH ($1.7444a_0 \leqslant R_{O-H} \leqslant 1.9444a_0$) and the center of the bond fixed at the origin. Contours are equally spaced by $0.02E_h$, starting at $-0.3704E_h$.

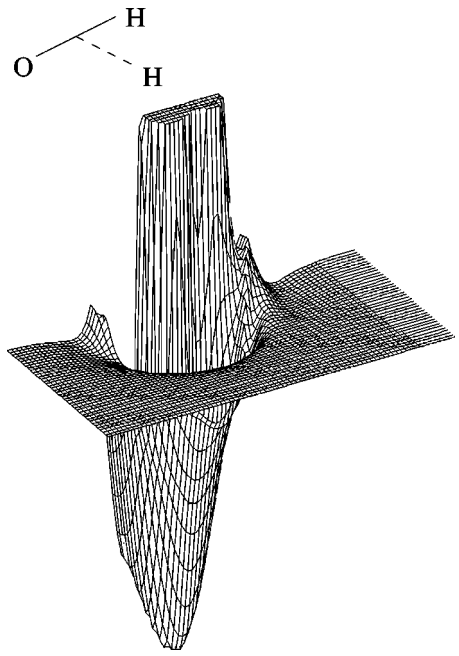

FIG. 9. Perspective view of H_2O ($X\,^1A'$) new PES, for H atom moving around an OH ($1.7444a_0 \leqslant R_{O-H} \leqslant 1.9444a_0$).

crossing with the ($^1\Sigma^+$) surface, and it is not apparent in Fig. 7.

Another interesting view of this surface is the approach of a $O(^1D)$ atom to an equilibrium $H_2(^1\Sigma_g^+)$ shown as a contour plot in Fig. 13 and in a perspective view in Fig. 14. This approach plays an important role on the reaction $O(^1D)+H_2(^1\Sigma_g^+) \rightarrow OH(^2\Pi)+H(^2S)$. The main feature we can see in this figure is the null activation barrier of this approach. The special contours give us a closer view where we can see a small van der Waals minimum and a small saddle point under the dissociation limit for the C_{2v} insertion, points (3) and (4) of Table XI.

In the work of Walch and Harding,[23] they obtained a smaller barrier (<0.2 kcal/mol) to collinear addition ($^1\Sigma^+$ surface) and did not find a barrier to edge-on insertion ($^1A'$ ground-state water surface), which is in agreement with our results.

VI. PRELIMINARY STUDIES OF THIS PES

We have done same preliminary studies in order to test the PES here presented. We present a QCT study at 300 K, where we compare these results with experimental data obtained from the literature and other surfaces. Those preliminary studies allow us to survey some characteristics and the

TABLE XI. Geometries and energies of metastable minima and saddle points for the new surface.

Point[a]	R_1	R_2	R_3	∠HOH	V
(1)	3.5230500	1.7539662	1.7690838	180.0	−0.3187002
(2)	5.9690555	4.1150065	1.8540490	180.0	−0.1758476
(3)	1.41124	4.7430591	4.7430591	17.11119	−0.1036791
(4)	1.4132597	4.4834532	4.4834532	18.13621	−0.1036700

[a]Points (1), (2), and (4) correspond to saddle points.

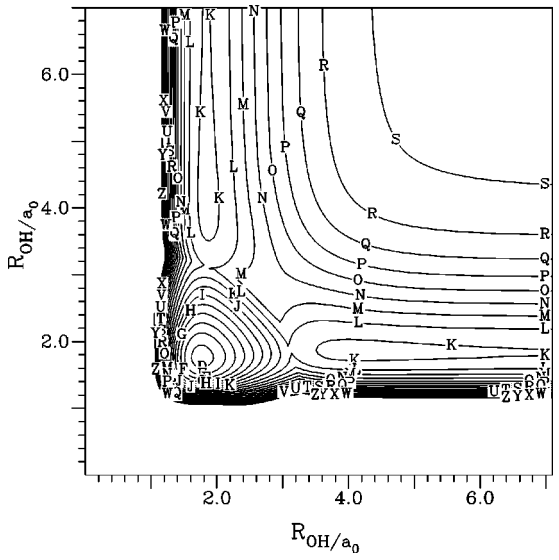

FIG. 10. Contours for collinear H–O–H geometries of the H_2O ground state. The asymptotic channel is $OH(^2\Pi)+H$. Contours are equally spaced by $0.02E_h$, starting at $-0.3704E_h$.

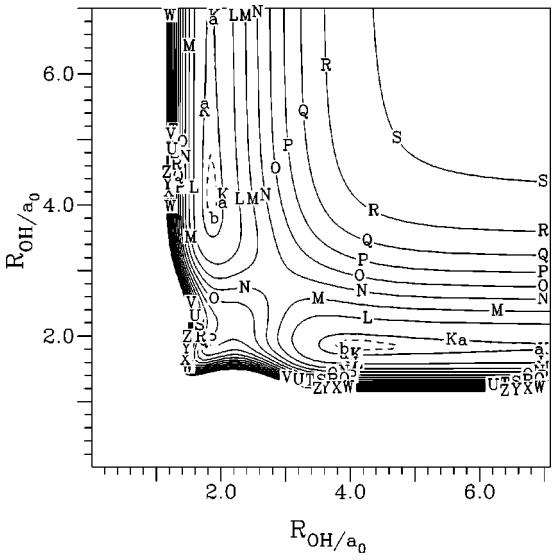

FIG. 12. Contours for the term V_2 $H_2O(^1\Pi)$ at the same geometry as in Fig. 10. The asymptotic channel is $OH(^2\Pi)+H$. Contours are equally spaced by $0.02E_h$, starting at $-0.3704E_h$.

quality of this new potential energy surface for H_2O molecule, in particular the long-range region that should play an important role in this reaction. Although we have not used spectroscopic information in the fitting procedure, we have also done a vibrational spectroscopic study to compare the predictions of our PES with others and experiment.

A. QCT study at 300 K

The $O(^1D)+H_2(^1\Sigma_g^+)\rightarrow OH(^2\Pi)+H(^2S)$ reaction is believed to have a null activation barrier. So the long-range forces between the O atom and the H_2 diatomic should play an important role on the dynamics of this important reaction in atmospheric and combustion chemistry.

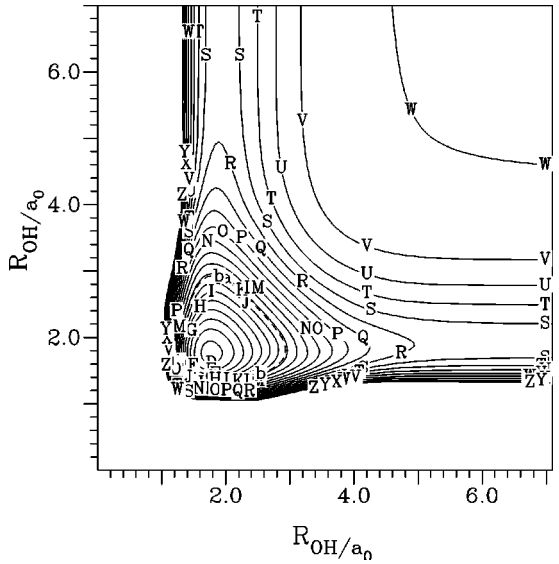

FIG. 11. Contours for the term V_1 $H_2O(^1\Sigma^+)$ at the same geometry as in Fig. 10. The asymptotic channel is $OH(^2\Sigma^+)+H$. Contours are equally spaced by $0.02E_h$, starting at $-0.3704E_h$.

The thermal rate constant at 300 K, for which there are more accurate data in literature has been computed using quasiclassical trajectory dynamic studies on the new H_2O potential energy surface. It has been shown that due to the electrostatic coupling between the Σ and Π states of lower energy at linear configurations, higher surfaces should contribute about 10% (Ref. 29) to the cross section at this temperature.

Using a batch of 5000 trajectories we estimate for the thermal rate constant a value of $0.999\pm0.024\times10^{-10}$ $cm^3\,molecule^{-1}\,s^{-1}$. Taking into account that correction we estimate the value of 1.1×10^{-10} $cm^3\,molecule^{-1}\,s^{-1}$, in excellent agreement with the recommended values for $k(300\ K)\times10^{10}$ (in $cm^3\,molecule^{-1}\,s^{-1}$) of 1.1 ± 0.1 (Ref. 30), 1.2 ± 0.1 (Ref. 31), and 1.1 ± 0.1 (Ref. 32) (for a range of temperatures between 200 K and 350 K). Comparing with results from other potential energy surfaces, we found in the literature several values for that rate constant at the same

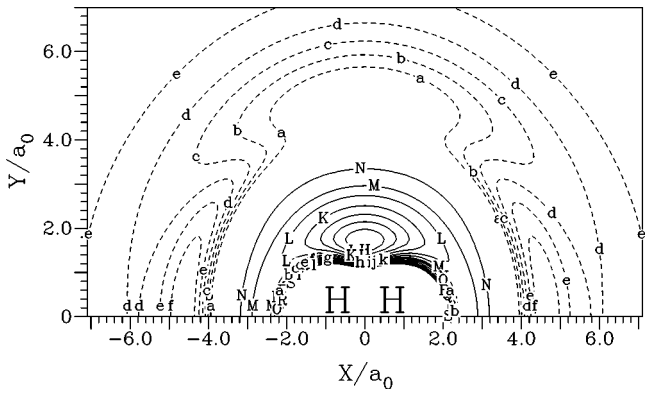

FIG. 13. Contour plot of H_2O ($X\ ^1A'$) new PES, for O atom moving around an H_2 ($1.311a_0 \leq R_{H-H} \leq 1.511a_0$) and the center of the bond fixed at the origin. Contours are equally spaced by $0.02E_h$, starting at $-0.3704E_h$; dashed contours are equally spaced by 0.1 kcal/mol, the contour labeled by f corresponds to the dissociation energy.

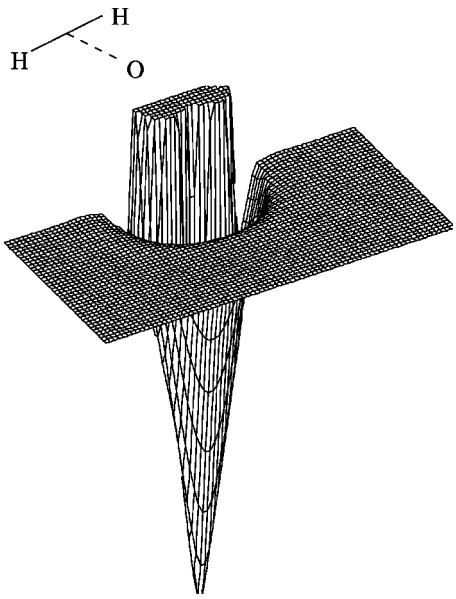

FIG. 14. Perspective view of H_2O ($X\,^1A'$) new PES, for O atom moving around an H_2 ($1.311a_0 \leqslant R_{H-H} \leqslant 1.511a_0$).

temperature. In particular, we quote for $k(300\ \mathrm{K}) \times 10^{10}$ the values of 0.843 in the PES of Schinke and Lester,[33] 1.63 in the PES of Varandas *et al.*,[8] and 1.3 in the work of Schatz *et al.*[34] (in $\mathrm{cm}^3\,\mathrm{molecule}^{-1}\,\mathrm{s}^{-1}$. Note that those results do not include any contribution from the excited states.

B. Spectroscopic study

We used our PES to carry out some spectroscopic calculations using the DVR3D suite of programs.[16] For this system, H_2O, we used Radau coordinates,[35,36] which are the appropriate coordinates for the *ABC* molecule, where one atom is bigger than the other two.

In Table XII we compare the calculated vibrational levels using our PES and using two versions of the potential from Partridge and Schwenke[4] (PS1 and PS2) and the potential of Polyansky, Jensen, and Tennyson[2] (PJT). Those results have been compared to the experimental values obtained in the literature. In conventional notation, ν_1, ν_2, and ν_3 represent the symmetric stretching, bending, and antisymmetric stretching, respectively.

Note that the PJT and PS2 potentials have been fitted to accurate spectroscopic data and our PES as well as PS1 use only *ab initio* data. In the vibrational calculations on the PS potentials we use the nuclear masses similar to Partridge and Schwenke and in the other calculations we use the atomic masses.

Table XII shows the reasonable results we have obtained with this new potential. This is due to the good quality of the *ab initio* points used and to the quality of the fitting in the region close to the bottom well.

TABLE XII. Vibrational levels for different PES of the water molecule.

Level	This work[a]	PJT[a]	PS1[a,b]	PS2[a,c]	Expt.[d]
010	1599.10	1594.68	1597.74	1594.79	1594.74635
020	3165.31	3151.56	3157.80	3151.69	3151.63015
100	3665.28	3657.15	3652.24	3657.08	3657.05325
030	4689.00	4666.61	4676.25	4666.56	4666.7931
002	7446.12	7444.75	7432.60	7445.19	7445.0700

[a]Calculated in this work.
[b]Only considered the *ab initio* fit.
[c]Considered the total fit.
[d]References 19–22 of Ref. 37.

VII. CONCLUSIONS

The main objective of this work was to build a PES for the water molecule in its fundamental state, $H_2O(X\,^1A')$. In this PES we take into account all the dissociation channels allowed by spin symmetry correlation, using the long-range interactions previously defined,[9] including the atom–diatom anisotropy and their dependence on the diatom coordinate. For the regions of strong interaction we have used *ab initio* data available in the literature.

We have attributed the *ab initio* data to the V_1 and V_2 diabatic surfaces in regions far from the crossing and to the V_X and V_B adiabatic surfaces in regions where the coupling term should play an important role. It has been necessary to carry out *ab initio* calculations for some geometries where the existing information was missing. The two adiabatic surfaces have been obtained in a global fit to define V_1, V_2 and the coupling term V_{12} in a total of 148 parameters.

We have performed quasiclassical trajectories studies in order to assess the importance of the long-range interactions carefully implemented in this PES. The close agreement with experiment reinforces this idea. Calculations of the vibrational levels have been done using the new surface. These have been compared with the results on other surfaces and experiment. The agreement obtained owes its quality to the effectiveness of the *ab initio* points as well as to the fitting procedure.

ACKNOWLEDGMENT

This work was supported by JNICT under the PRAXIS/PCEX/C/QUI/102/96 research project.

[1] T.-S. Ho, T. Hollebeek, H. Rabitz, L. B. Harding, and G. C. Schatz, J. Chem. Phys. **105**, 10 472 (1996).
[2] O. L. Polyansky, P. Jensen, and J. Tennyson, J. Chem. Phys. **105**, 6490 (1996).
[3] A. J. C. Varandas, J. Chem. Phys. **105**, 3524 (1996).
[4] H. Partridge and D. W. Schwenke, J. Chem. Phys. **106**, 4618 (1997).
[5] A. J. C. Varandas, J. Chem. Phys. **107**, 867 (1997).
[6] A. J. Dobbyn and P. J. Knowles, Mol. Phys. **91**, 1107 (1997).
[7] A. J. C. Varandas, A. I. Voronin, and P. J. S. B. Caridade, J. Chem. Phys. **108**, 7623 (1998).
[8] A. J. C. Varandas, A. I. Voronin, A. Riganelli, and P. J. S. B. Caridade, Chem. Phys. Lett. **278**, 325 (1997).
[9] J. Brandão and C. M. A. Rio, Chem. Phys. Lett. **372**, 866 (2003).
[10] J. N. Murrell, S. Carter, I. M. Mills, and M. F. Guest, Mol. Phys. **42**, 605 (1981).
[11] A. J. C. Varandas, Adv. Chem. Phys. **74**, 255 (1988).
[12] T. H. Dunning, Jr., J. Chem. Phys. **90**, 1007 (1989).
[13] W. Kołos and L. Wolniewicz, J. Chem. Phys. **43**, 2429 (1965).
[14] W. Kołos and L. Wolniewicz, Chem. Phys. Lett. **24**, 457 (1974).
[15] R. J. Fallon, I. Tobias, and J. T. Vanderslice, J. Chem. Phys. **34**, 167 (1961).

[16] J. Tennyson, J. R. Henderson, and N. G. Fulton, Comput. Phys. Commun. **86**, 175 (1995).
[17] A. J. C. Varandas and J. Dias da Silva, J. Chem. Soc., Faraday Trans. **88**, 941 (1992).
[18] A. J. C. Varandas and J. Brandão, Mol. Phys. **45**, 857 (1982).
[19] R. J. Le Roy, *Specialist Periodical Report, Molecular Spectroscopy* (The Chemical Society, London, 1973), p. 113.
[20] M. W. Schmidt, K. K. Baldridge, J. A. Boatz *et al.*, J. Comput. Chem. **14**, 1347 (1993).
[21] A. J. C. Varandas and A. I. Voronin, Chem. Phys. **194**, 91 (1995).
[22] F. Schneider, F. D. Giacomo, and F. A. Gianturco, J. Chem. Phys. **104**, 5153 (1996).
[23] S. P. Walch and L. B. Harding, J. Chem. Phys. **88**, 7653 (1988).
[24] F. B. Brown and D. G. Truhlar, Chem. Phys. Lett. **117**, 307 (1985).
[25] R. A. Kendall, T. H. Dunning, Jr., and R. J. Harrison, J. Chem. Phys. **96**, 6769 (1992).
[26] S. F. Boys and F. Bernardi, Mol. Phys. **19**, 553 (1970).
[27] S. Farantos, E. C. Leisegang, J. N. Murrell, K. Sorbie, J. J. C. Teixeira-Dias, and A. J. C. Varandas, Mol. Phys. **34**, 947 (1977).
[28] J. S. Kain, O. L. Polyansky, and J. Tennyson, Chem. Phys. Lett. **317**, 365 (2000).
[29] K. Drukker and G. C. Schatz, J. Chem. Phys. **111**, 2451 (1999).
[30] W. B. DeMore, S. P. Sander, D. M. Golden, R. F. Hampson, M. J. Kurylo, C. J. Howard, A. R. Ravishankara, C. E. Kolb, and M. J. Molina, *Chemical Kinetics and Photochemical Data for Use in Stratospheric Modeling*, JPL Publication No. 97-4, NASA-Jet Propulsion Laboratory, 1997.
[31] R. K. Talukdar and A. R. Ravishankara, Chem. Phys. Lett. **253**, 177 (1996).
[32] R. Atkinson, D. L. Baulch, R. A. Cox, R. F. Hampson, Jr., J. A. Kerr, and J. Troe, J. Phys. Chem. Ref. Data **21**, 1125 (1992).
[33] R. Schinke and W. A. Lester, Jr., J. Chem. Phys. **72**, 3754 (1980).
[34] G. C. Schatz, A. Papaioannou, L. A. Pederson, L. B. Harding, T. Hollebeek, T.-S. Ho, and H. Rabitz, J. Chem. Phys. **107**, 2340 (1997).
[35] F. T. Smith, Phys. Rev. Lett. **45**, 1157 (1980).
[36] B. R. Johnson and W. P. Reinhadt, J. Chem. Phys. **85**, 4538 (1986).
[37] P. Jensen, S. A. Tashkun, and V. G. Tyuterev, J. Mol. Spectrosc. **168**, 271 (1994).